Astron. Astrophys. 280, 409–425 (1993)

ASTRONOMY AND ASTROPHYSICS

The distribution of ionized gas in early–type galaxies*

L.M. Buson[1], E.M. Sadler[2], W.W. Zeilinger[3], G. Bertin[4], F. Bertola[5], J. Danziger[6], H. Dejonghe[7], R.P. Saglia[8,9], and P.T. de Zeeuw[10]

[1] Osservatorio Astronomico, Padova, Italy
[2] Anglo-Australian Observatory, Epping, Australia
[3] ST–ECF, Garching bei München, Germany
[4] Scuola Normale Superiore, Pisa, Italy
[5] Dipartimento di Astronomia, Padova, Italy
[6] ESO, Garching bei München, Germany
[7] RUG Observatorium, Gent, Belgium
[8] Landessternwarte, Heidelberg, Germany
[9] Dipartimento di Matematica, Pisa, Italy
[10] Sterrewacht Leiden, The Netherlands

Received April 13, accepted July 27, 1993

Abstract. We present and discuss Hα+[N II] imaging observations of fifteen nearby elliptical and S0 galaxies with extended optical emission lines. The morphology of the emitting regions suggests that the ionized gas usually lies in a disk which is often geometrically decoupled from the stellar body, as expected in a triaxial galaxy. The presence of a gaseous disk makes these galaxies suitable for testing their gravitational field in a straightforward way.

The presence of dust in many of the disks, together with the observed morphological properties, suggests that the ionized gas in most of these galaxies is more closely associated with the cold ISM than with the hot X–ray component. The mass of ionized gas in the galaxies studied here is typically 10–100 times that in a 'normal' early–type galaxy of similar optical luminosity. These appear to be galaxies where an unusually high fraction of the cold gas has been ionized, rather than unusually gas–rich systems in an overall sense. The extra ionizing source may be related to an active nucleus, since the continuum radio emission from these galaxies is typically 10–15 times more powerful than in 'normal' ellipticals of the same optical luminosity.

Key words: galaxies: elliptical and lenticular, cD – galaxies: ISM – galaxies: structure

1. Introduction

It is now generally recognized that elliptical galaxies are not gas–free as was once thought, but have a rich and complex interstellar medium (ISM) quite different in character from that in spiral galaxies. Hot (10^7 K) X–ray gas usually dominates the ISM in luminous elliptical galaxies, but smaller amounts of warm (10^4 K) ionized gas, cold (< 100 K) atomic and molecular gas and dust are also commonly seen (e.g. Bregman et al. 1992; Macchetto & Sparks 1992 and references therein). Typical masses are 10^8–$10^{10} M_\odot$ for the X–ray gas, 10^2–$10^4 M_\odot$ in ionized gas and 10^6–$10^8 M_\odot$ in cold atomic and molecular gas (Roberts et al. 1991; Phillips et al. 1986, hereafter PJDSB).

While the typical amount of hot (X–ray) ISM, which appears to be unique to luminous early–type galaxies (Fabbiano 1989), depends strongly on the optical luminosity ($L_X \propto L_B^{1.75}$, White & Sarazin 1991; Bregman et al. 1992), the HI content (Knapp et al. 1985), dust content (Forbes 1991) and CO content (Lees et al. 1991) are unrelated to the stellar luminosity, in contrast to the case for spiral galaxies. As a consequence, Bregman et al. (1992) suggest that the hot ISM is a bulge–related phenomenon and the cold component (atomic and molecular gas and dust) is disk–like, with little interaction between the two.

The warm ionized component, though less massive than the hot and cold components of the ISM, is nevertheless extremely common. Analysis of the PJDSB data with the ASURV survival analysis package (LaValley et al. 1992; implementing the methods discussed by Feigelson & Nelson 1985 and Isobe et al. 1986) shows that 70% of bright ($M_B < -20$) early–type galaxies have Hα+[N II] emission line luminosities of at least 10^{39} erg/s (roughly corresponding to an ionized gas mass of $10^3 M_\odot$ for $H_0 = 55$ km/s/Mpc). In these galaxies the typical emission–line luminosity correlates strongly with the stellar luminosity ($L_{em} \propto L_B^{1.03\pm.15}$), suggesting a link with the hot ISM as might be expected in a cooling flow picture (e.g. Thomas et al. 1986).

Send offprint requests to: L.M. Buson, Osservatorio Astronomico di Padova, Vicolo dell'Osservatorio 5, I-35122 Padova, Italy

* Based on observations collected at the European Southern Observatory, La Silla (Chile).

On the other hand, several pieces of evidence suggest that in elliptical galaxies (and possibly also many S0 galaxies; Bertola et al. 1988; 1992a) both the warm gas and dust and the cold component have been accreted from outside in an interaction or merging event. The most direct evidence for this hypothesis is the observation that the rotation axes of gas disks in early–type galaxies are frequently misaligned with (or even perpendicular/counter to) those of the underlying stellar component (Bertola 1987; Bertola et al. 1992a).

Although in individual cases the morphology, orientation and kinematics of the ionized gas may provide important clues to its origin, existing data are still largely incomplete and our understanding of the origin of the warm (10^4 K) component remains fragmentary. Hα imaging of X–ray selected samples of galaxies led both Heckman et al. (1989) and Trinchieri & di Serego Alighieri (1991, hereafter TdiSA) to conclude that the luminosity of Hα emission ($L_{\rm em}$) correlated with the amount of X–ray gas present. In contrast, Shields (1991) also observed an X–ray selected sample and found that $L_{\rm em}$ was uncorrelated with X–ray luminosity but did correlate with the far–IR luminosity which traces the cold gas component. It seems likely that in some galaxies (particularly central galaxies in X–ray clusters like those studied by Heckman et al. 1989) the ionized gas comes largely from the X–ray halo, while in others it is associated with cold gas which may have been recently captured, so the results of statistical studies depend strongly on how the galaxies are selected. Even in the central galaxies of X–ray clusters, however, some cold gas may have been captured in a merger (e.g. Sparks et al. 1989).

Clearly more imaging data for 'normal' galaxies are needed for a complete picture to emerge. At least 25% of the galaxies in which emission lines are detected have ionized gas extending 2 kpc or more from the nucleus (PJDSB), so that full two–dimensional coverage is essential to determine the total extent and luminosity of the ionized component. Imaging data of this kind are still sparse, and many of the objects which have been observed to date are powerful radio galaxies or the brightest members of clusters, rather than 'normal' systems. The present lack of data is also reflected in the recent catalogue of Roberts et al. (1991) who give extensive and quantitative data on the X–ray, HI and dust properties of a sample of 467 'normal' early–type galaxies, but confine their discussion of ionized gas to noting the presence or absence of emission lines in optical spectra.

Here we use emission–line images to measure the distribution, luminosity and mass of ionized gas in fifteen nearby elliptical and S0 galaxies already known to show emission lines of Hα and [NII] in their optical spectra. A few objects included in our sample also show dust features in their optical images. In this respect, it is important to recognize that 'dust–lane' ellipticals (i.e. those which show regular, well–defined absorption rather than diffuse filaments or patches of dust) are only a favourably–oriented sub–class of elliptical galaxies with gas disks. A disk seen within about $10 - 15°$ of edge–on appears as a dust lane crossing the stellar body of an otherwise normal elliptical galaxy (Bertola & Galletta 1978; Hawarden et al. 1981; Ebneter & Balick 1985; Bertola 1987, 1992). A randomly–oriented gas disk is more difficult to recognise, and can usually be detected only by the emission lines which arise from ionized gas associated with the dust, i.e. by emission–line imaging or spectroscopy. However, it should be noted that the morphology of the emission–line gas can be either regular (flattened or round in shape) or filamentary, showing arcs, strings and other peculiar features (Baum et al. 1988; Macchetto & Sparks 1992, Sparks et al. 1993). Only kinematic data can provide a decisive test of whether the gas in an individual galaxy lies in a disk with ordered rotation.

Indeed, studies of the velocity field of the ionized gas in 'normal' early–type galaxies are generally consistent with a disk rotating about the nucleus (e.g. Demoulin–Ulrich et al. 1984, hereafter DBB; PJDSB; Bertola et al. 1991), and ordered rotation usually dominates over turbulent motions even for very active galaxies in which radio jets may pass through the disk (Baum et al. 1989). As a consequence, the presence of such disks gives us a powerful tool to investigate the gravitational field of the underlying galaxy. The observations described here are part of an ESO Key Program (Bertin et al. 1989; Amico et al. 1993) in which we aim to determine the mass–to–light ratios of nearby elliptical galaxies.

In Sect. 2 we present the observations and describe the data reduction. We consider the morphology of the resulting images in Sect. 3, and discuss the physical conditions of the ionized gas in Sect. 4. We summarize our conclusions in Sect. 5.

2. Observations and reduction

2.1. Selection of the galaxies

The 15 galaxies in Table 1 were chosen because they were already known to show extended optical emission lines. Since, as noted above, our original aim was to identify suitable objects for a study of the kinematics of the gas, this is in no way a complete sample. Eight of the galaxies are members of the complete sample south of declination $-35°$ studied by PJDSB and the other seven are more northerly objects selected from the literature. In contrast to other imaging studies (Kim 1989; Shields 1991; TdiSA), the galaxies were not chosen on the basis of their X–ray or IRAS fluxes.

2.2. Observations

Direct imaging data analysed in the present work come from two observing runs at the ESO/MPI 2.2-m telescope, on March 6–7 and Oct. 27–Nov. 1 1989. Table 1 gives the observing log. The detector was a high resolution 1024 × 640 pixel RCA CCD (ESO CCD#11) with 15 μm pixels. The scale is 0.176 arcsec pixel^{-1} unbinned, but in the first run we used a 2×2 pixel binning, giving a scale of 0.352 arcsec pixel^{-1}. The field of view of the CCD was 3.0 × 1.9 arcmin^2. Weather conditions were photometric for most of the observing time. The seeing ranged from 1.0 to 1.7 arcsec FWHM.

As a rule, four images (two in the redshifted Hα line and two in the adjacent continuum) were obtained for each galaxy, with exposure times ranging from 20 min to 45 min per image. Spectrophotometric standard stars included in the list of Oke

Table 1. Log of observations

Object	RSA Type[a]	RC3 Type[b]	B_T^c	cz[d] km s^{-1}	Exp. T.[e] min	Hα/Cont.[f] filter	Seeing arcsec
NGC 484		$SA0^-$	13.1	5200	20+45	390/1601	1.0
NGC 745		$S0^+$pec	14.0	5953	40	390/1601	1.6
NGC 1395	E2	E2	10.5	1699	20+45	388/1601	1.0
NGC 1453	E0	E2-3	12.6	3933	20+45	389/1601	1.0
ESO 118–G34		$S0^0$pec	13.5	1171	30	388/1601	1.5
NGC 1947	$S0_3(0)$pec	$S0^-$pec	11.6	1157	20+45	388/1601	1.6
NGC 2974	E4	E4	11.9	2006	18+18	388/390	1.1
NGC 3962	E1	E1	11.6	1818	25+25	388/390	1.1
NGC 4636	$E0/S0_1(6)$	E0-1	10.4	927	40+45	388/390	1.5
NGC 5846	$S0_1(0)$	E0-1	11.0	1710	17.5	388/390	1.3
NGC 6868	$E3/S0_{2/3}(3)$	E2	11.7	2858	20+20	388/1601	1.3
ESO 234–G21		$SA0^0$pec	13.9	5430	20	390/1601	1.7
NGC 7097	E4	E5	12.6	2539	20+45	388/1601	1.0
NGC 7302	$S0_1(4)$	$SA(s)0^-$	13.2	2586	20	388/1601	1.6
IC 1459	E4	E	11.0	1691	15	388/1601	1.3

Notes:
a Morphological type from the *Revised Shapley-Ames Catalog of Bright Galaxies* (RSA; Sandage & Tammann 1987).
b Morphological type from the *Third Reference Catalogue of Bright Galaxies* (RC3; de Vaucouleurs et al. 1991).
c Total B magnitude; from RC3.
d Heliocentric radial velocity; from RC3.
e Exposure times in the line and continuum filter (purposely the same).
f ESO Filter Inventory number (Gilliotte 1990).

(1974) were also recorded for calibration purposes. Depending on each galaxy's redshift, we used one of three redshifted Hα interference filters. Table 2 lists the filter specifications. The filter numbers refer to the ESO Filter Inventory (Gilliotte 1990). The on–band filters usually included emission both from Hα and [NII] λλ 6548, 6584 Å with the exception of NGC 6868, NGC 7097 and NGC 7302 where the [NII] λ 6584 Å line falls partially outside the filter passband.

Table 2. Filter specifications

Filter[a]	$\lambda_{central}$ (Å)	Δλ (Å)	Trans. (%)	Notes
388	6597	77	86	Hα set
389	6642	80	83	Hα set
390	6678	80	88	Hα set
1601	6449	61	74	Continuum

Notes:
a ESO Filter Inventory number (Gilliotte 1990).

2.3. Data reduction

Basic reduction and analysis were done in Padova and ESO–Garching with the MIDAS software package. Each frame was bias–subtracted and corrected for dark counts, then flat fielded using a normalized dome flat of the corresponding filter and corrected for atmospheric extinction. Pairs of images obtained through the same filter were aligned (to better than 0.2 pixel) using the brightest stellar images in the field as a reference, then averaged to give a single image. The averaging routine, rejecting differences higher than the noise level, also removed cosmic ray hits from the images. After subtracting the sky contribution (estimated from a portion of the frame not significantly contaminated by galaxy light), we subtracted the continuum image, properly aligned and scaled to allow for transmission differences between the filters, from the image obtained with the line filter to give a pure emission–line image.

To derive a starlight–free final image, the rescaling parameter for the continuum frame must be carefully determined. A first estimate can be obtained from the observed count rates of a standard star in the two filters and its expected fluxes at those wavelengths, and this should account for the relative efficiencies of telescope, filters and detector in the two bands. However, a correct estimate is hampered by the poorly known energy distribution of the observed standard stars as well as by the intrinsic weakness of emission lines relative to the continuum in most of these galaxies. As a consequence, additional fine–tuning of the scaling parameter is needed to see the faintest structures. We chose the final scaling factor so as to subtract the maximum amount of continuum without producing spurious negative features in the resulting subtracted images shown in Fig. 1. Though these images show no emission in regions lacking structured

Table 3. Geometrical parameters of stars and gas in 13 galaxies

Object	PA_{stars} deg.	PA_{gas} deg.	ϵ_{stars}	ϵ_{gas}	i_{disk} deg.	Radius arcsec	ΔPA deg.
NGC 484	89	97	.20	.25	41	2–4	8
NGC 745	33	47	.17	.31	46	2–5	14
NGC 1395	86	93	.11	.28	44	2–3	7
NGC 1453	28	152	.15	.29	45	2–4	56
NGC 2974	39	59	.29	.48	59	3–6	20
NGC 3962	8	49	.17	.41	54	3–7	41
NGC 4636	159	108	.03	.32	47	5–11	51
NGC 5846	85		.07			5–10	
NGC 6868	80	28	.13	.42	54	3–5	52
ESO 234–G21	160	139	.18	.48	59	2–4	21
NGC 7097	19	169	.21	.46	57	2–4	30
NGC 7302	92	87	.07	.33	48	1–3	5
IC 1459	33	46	.23	.36	50	3–6	13

ionized gas, they could "conceal" an extended faint component and the derived fluxes should be regarded as lower limits.

2.4. Analysis of the emission–line and continuum images

The pure emission–line images were analysed at the AAO with the GRASP surface photometry program (Jedrzejewski 1987) to determine the major axis position angle (PA), ellipticity and surface brightness profile of the gas component in each galaxy. They are shown in Fig. 2 as a function of the major–axis distance from the center. The surface brightness profiles are flux calibrated by means of standard star observations, in terms of AB magnitude in the passband of the adopted filter (Oke 1974)[1].

Owing to the uncertainty in the energy distribution of the standard stars, these profiles may be affected by systematic errors as large as ± 0.5 magnitudes. Due to the irregular morphology of the outer gas, the region where the isophotes can be fitted accurately is usually smaller than the region where the emission can be detected. The geometrical parameters listed in Table 3 refer to the largest radii where the gas isophotes are well described by ellipses.

Two galaxies have been excluded from this analysis: NGC 1947, where the prominent dust lane obscures much of the stellar body, and ESO 118–G34, an HII region–rich galaxy whose gas morphology is quite different from the others in the sample. Furthermore, the inner region of the gaseous disk of NGC 4636 has also been excluded, owing to the presence of an asymmetric ring feature, while for NGC 5846, whose gas component has a complex morphology not suitable for fitting the isophotes by ellipses, only the star component profiles have been derived.

The total Hα+[NII] emission–line flux was derived from our standard star observations following the procedure described by di Serego Alighieri (1990), by assuming the sensitivity, filter transmission and star absolute flux are constant across the filter bandwidth. The resulting fluxes are given in Table 4 together with computed luminosities within the same aperture. Adopted distances are from the "220 model" of Kraan–Korteweg (1986), assuming a Virgo Cluster distance of 21.7 Mpc. Since the model adopts an infall velocity towards Virgo of 220 km s^{-1} and a Virgo Cluster observed redshift of 967 km s^{-1}, this corresponds to a Hubble constant of H_0 = 55 km s^{-1} Mpc^{-1} in an unperturbed velocity field.

Table 5 compares our measured emission–line flux with the total Hα+[NII] flux measured by other observers for six galaxies of our sample. Shields (1991) gives a detailed error analysis for the continuum subtraction method used here, and concludes that while flat–fielding and continuum scaling are the major uncertainties for fluxes measured at small radii, flux measurements for galaxies with very extended emission can be subject to severe systematic effects. As a result, objects such as NGC 5846, an example of a galaxy with weak extended emission, can have a large spread in measured $f_{H\alpha+[NII]}$ for different observers. Moreover, the few objects of our sample whose [NII] λ 6584 Å emission line is not fully included in the filter passband, can lose a fraction as high as 50% of the total Hα+[NII] flux, if we assume that the [NII] λ 6584 and Hα emission lines are of comparable intensity. Thus, on the basis of both internal and systematic uncertainties, it seems realistic to assume that our flux measurements are typically accurate to within a factor of two.

The continuum images were analysed both with GRASP and with the ELLFIT ellipse fitting procedure of Bender & Möl-

[1] No usable standard star observations were available for the night of Mar. 7; calibrated surface brightness profiles as well as Hα fluxes of NGC 3962, NGC 4636 and NGC 5846 have been derived from calibration frames of the previous night.

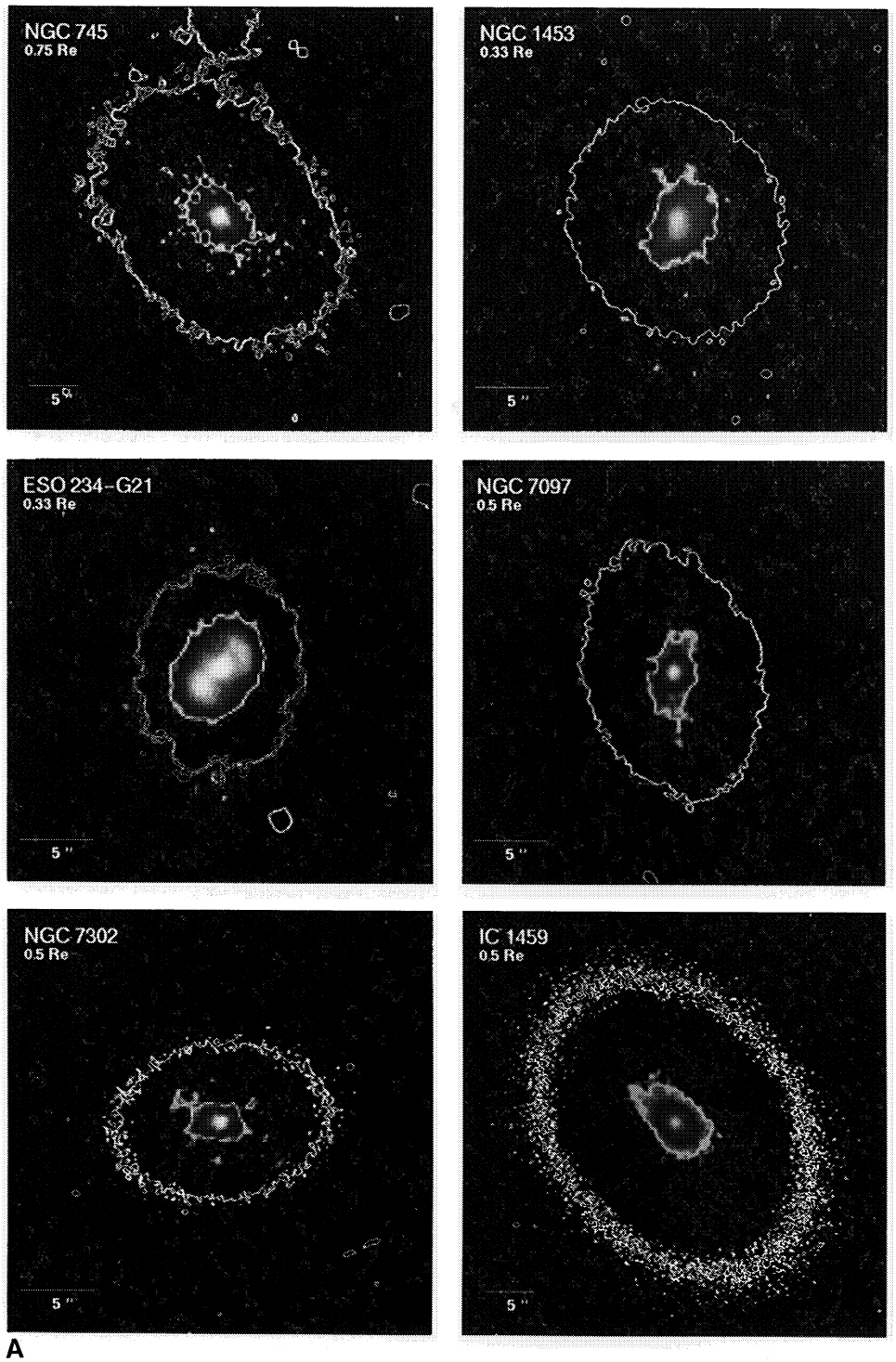

Fig. 1. a–d. Continuum and line emission images of the 15 early–type galaxies in our sample. Emission–line images are displayed in a logarithmic intensity scale. Plate **a** shows the Hα+[NII] line emission images of NGC 745, NGC 1453, ESO 234-G21, NGC 7097, NGC 7302 and IC 1459. Sumperimposed on each image is a selected continuum isophote in order to show the shape and orientation of the galaxy body; the distance along the major axis is displayed below the identification in units of B-band effective radii from the RC3 (de Vaucouleurs et al. 1991). The left hand panels of plates **b**, **c** and **d** display in the same way the emission images of the remaining objects while the respective right hand panels show details of the continuum light images. For NGC 484, NGC 1395, NGC 1947, NGC 3962, NGC 4636, NGC 5846 and NGC 6868 the residuals after subtraction of a smooth galaxy model are shown (the darker areas indicate absorption due to dust). Line emission isophotes are superimposed on the continuum image of ESO 118–G34 in order to reveal the partly different nature of continuum and line emission knots. For NGC 2974 the resulting continuum image after application of the adaptive filter is shown (see Sect. 2.4)

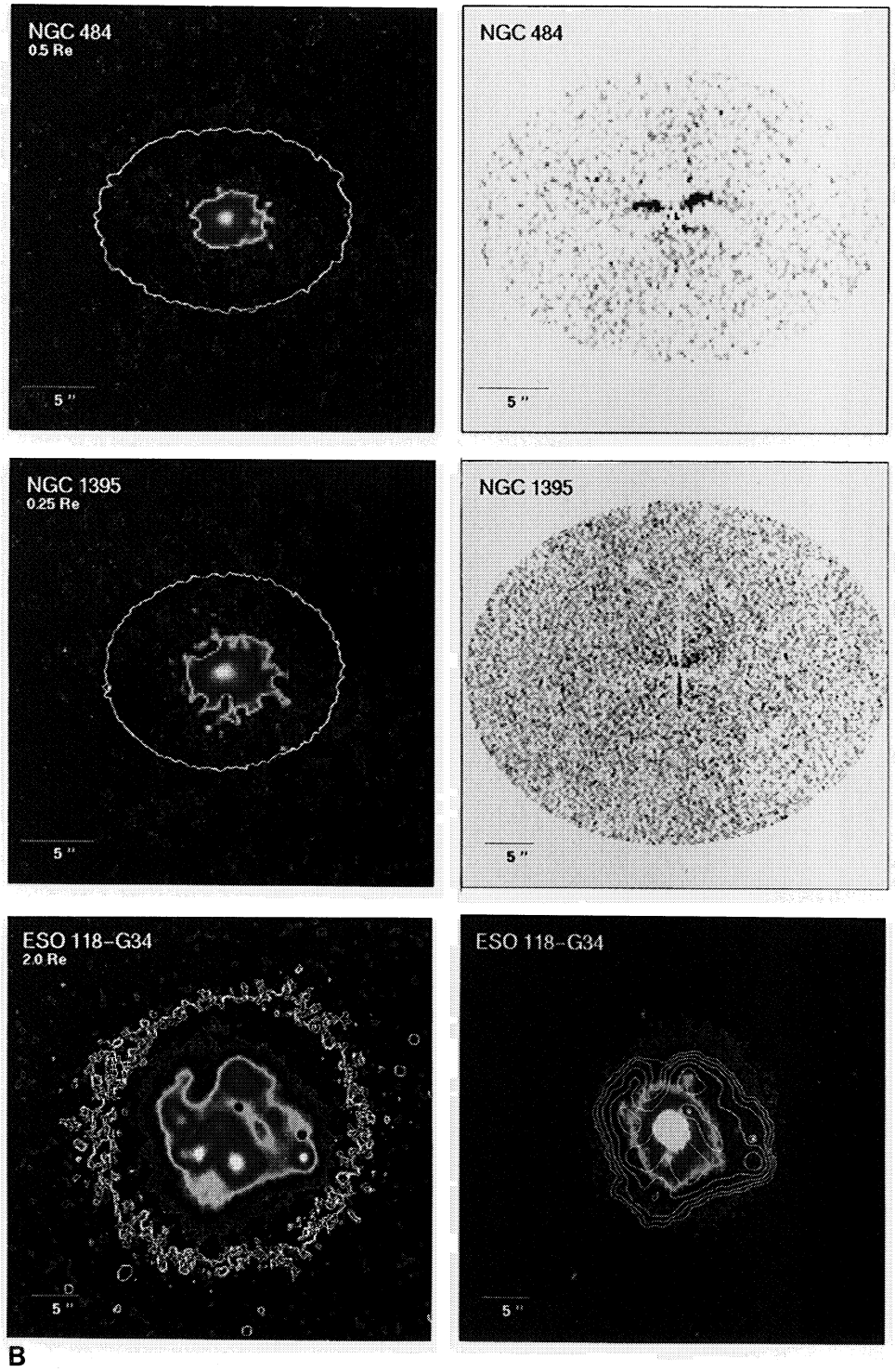

Fig. 1. (continued)

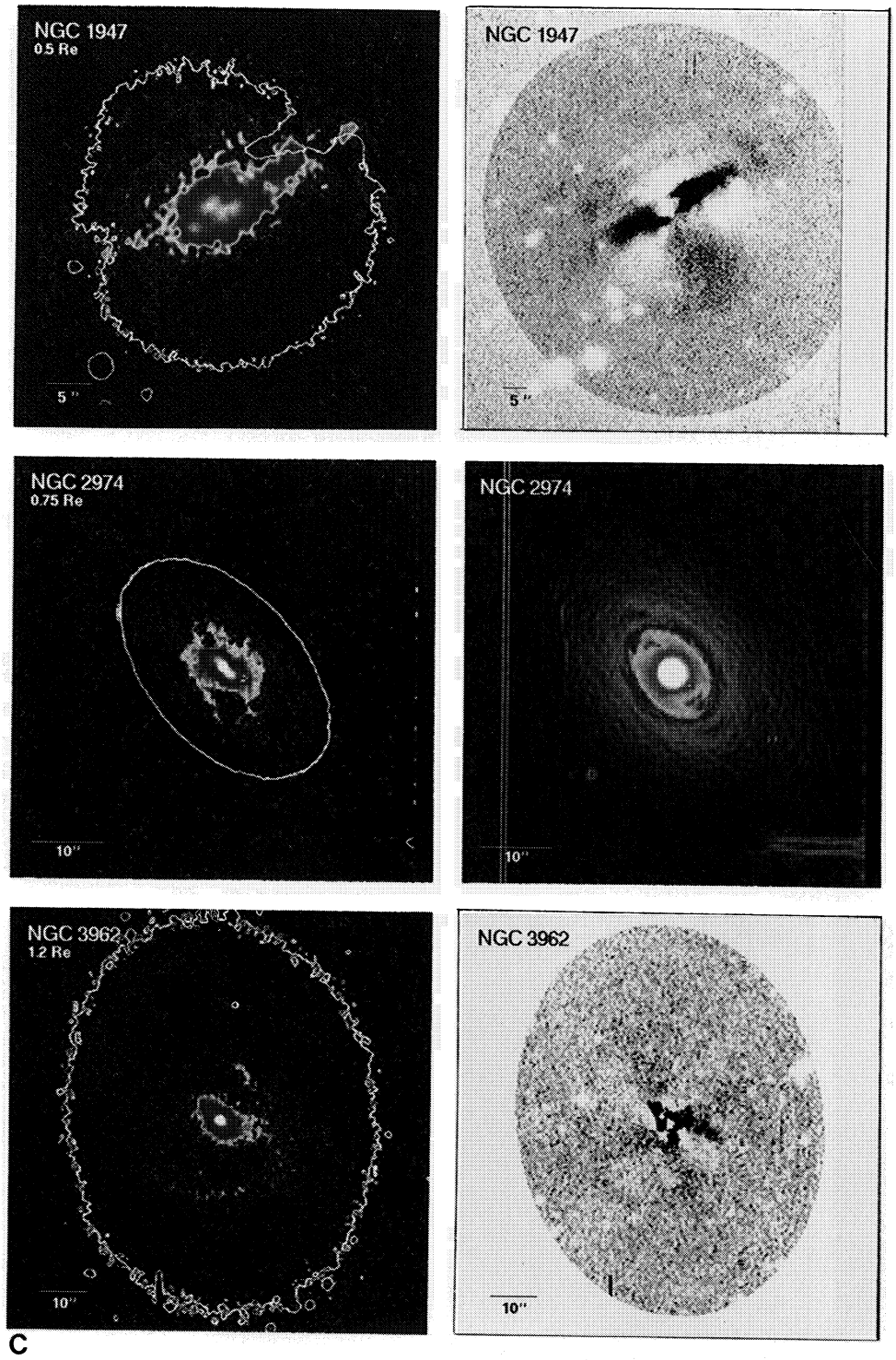

Fig. 1. (continued)

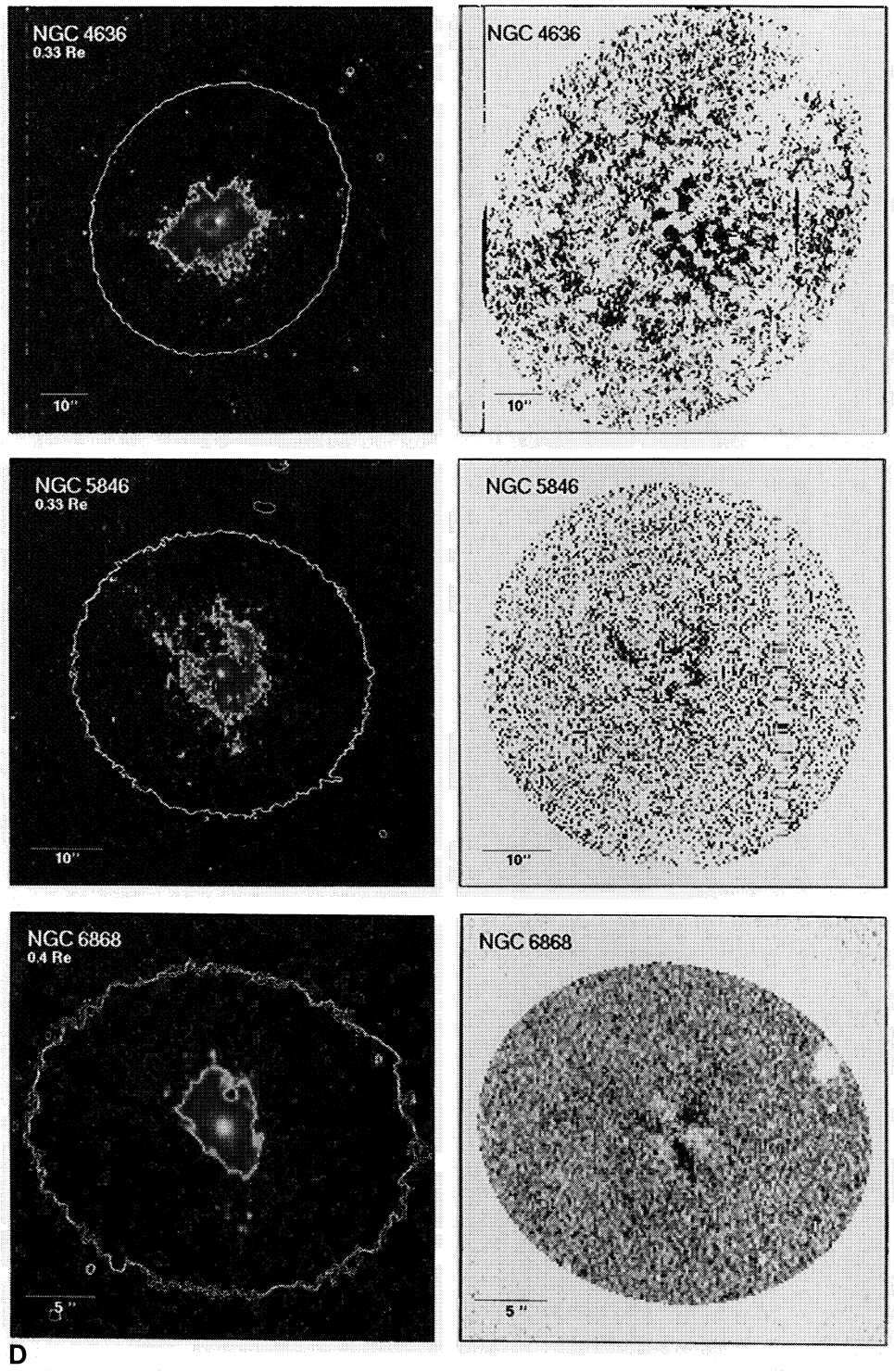

Fig. 1. (continued)

Table 4. Hα + [NII] fluxes and luminosities for program galaxies

Object[a]	D Mpc	A_B^b mag	Radius[c] arcsec	$f_{H\alpha+[NII]}$ erg cm^{-2} s^{-1}	$L_{H\alpha+[NII]}$ erg s^{-1}
NGC 484	90.1	0.00	9.7	2.1×10^{-13}	2.0×10^{41}
NGC 745	103.9	0.00	5.5	4.5×10^{-14}	5.8×10^{40}
NGC 1395	29.7	0.02	7.5	5.2×10^{-14}	5.5×10^{39}
NGC 1453	71.2	0.25	7.5	1.7×10^{-13}	1.2×10^{41}
ESO 118–G34	18.7	0.00	10.3	9.9×10^{-13}	4.1×10^{40}
NGC 1947	19.3	0.16	11.3	1.3×10^{-13}	6.3×10^{39}
NGC 2974	38.8	0.12	10.7	2.0×10^{-13}	3.8×10^{40}
NGC 3962	36.2	0.04	28.3	1.7×10^{-13}	2.7×10^{40}
NGC 4636	21.7	0.05	17.7	2.2×10^{-13}	1.3×10^{40}
NGC 5846	36.7	0.15	15.1	1.7×10^{-13}	3.0×10^{40}
NGC 6868[#]	48.8	0.15	8.4	1.0×10^{-13}	3.1×10^{40}
ESO 234–G21	96.8	0.09	10.4	4.2×10^{-13}	4.9×10^{41}
NGC 7097[#]	45.3	0.00	5.8	6.1×10^{-14}	1.5×10^{40}
NGC 7302[#]	47.5	0.19	4.2	3.7×10^{-14}	1.1×10^{40}
IC 1459	29.5	0.04	8.4	4.6×10^{-13}	4.9×10^{40}

Notes:
a [#] indicates that the line λ [NII] 6584 Å falls partly outside the filter passband.
b Galactic extinction in the B band from RC3.
c Circular aperture radius covering the whole area of line emission.

Table 5. Comparison of our flux measurements with those of other observers

Galaxy	$f_{H\alpha+[NII]}$ (erg cm^{-2} s^{-1}) *This paper*	*Other obs.*	*Reference*
NGC 1395	5.2×10^{-14}	$<9.1 \times 10^{-14}$	Shields[a]
		2.3×10^{-13}	TdiSA
NGC 2974	2.0×10^{-13}	1.8×10^{-13}	Shields
		3.1×10^{-13}	Kim
NGC 4636	2.2×10^{-13}	1.1×10^{-13}	Shields[b]
NGC 5846	1.7×10^{-13}	$<8.7 \times 10^{-14}$	Shields
		5.4×10^{-13}	TdiSA
NGC 6868	1.0×10^{-13}	1.0×10^{-13}	Hansen et al. 1991.
IC 1459	4.6×10^{-13}	8.2×10^{-13}	Shields
		1.2×10^{-12}	Goudfrooij et al. 1990

Notes:
a Within 6.8 arcsec radius.
b Within 8 arcsec radius. Shields also measures an upper limit of $<2.1 \times 10^{-13}$ erg cm^{-2} s^{-1} within a 16 arcsec radius, which is consistent with our measurement.

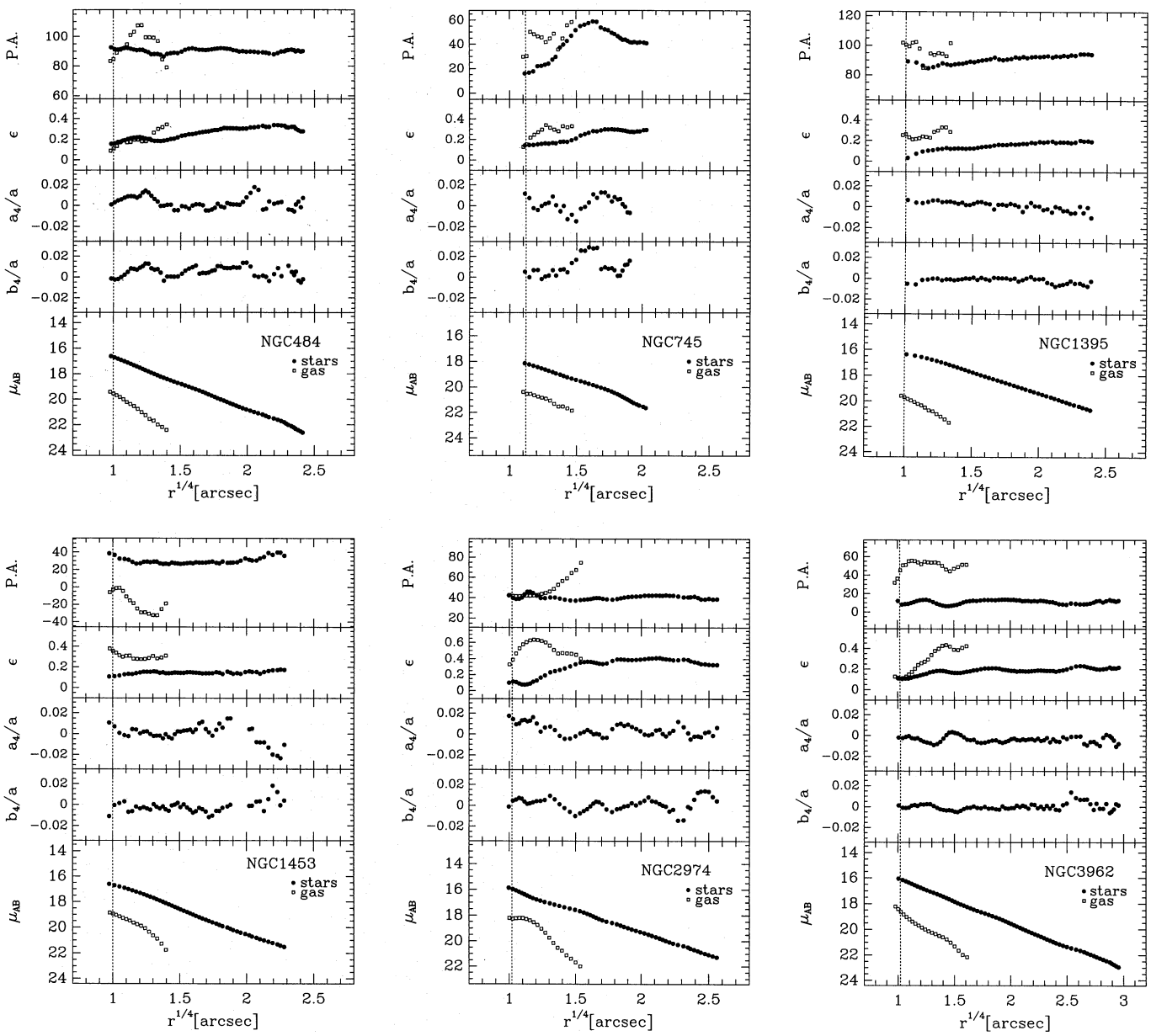

Fig. 2. a–m. Surface brightness, major axis position angle and ellipticity profiles as a function of the major–axis distance from the centre for stars and gas of the galaxies in Table 3. The radial profiles of the parameters a_4 and b_4 for the stellar component are shown also. The value of the seeing is indicated by the vertical dashed line. Owing to the anomalous morphology of the emitting region, the whole gaseous component of NGC 5846 and the inner gaseous disk of NGC 4636 were excluded from this figure.

lenhoff (1987). (The latter also measures the a_4 and b_4 terms which describe the deviations of the isophotes from pure ellipses). The surface brightness profiles were flux calibrated as described above, and there was very good agreement between P.A., ellipticity and surface brightness profiles derived by the two packages. The resulting ELLFIT profiles are shown in Fig. 2 and the derived parameters listed in Table 3.

In order to look for substructure, we used the best fitting profiles to construct a smooth model for each galaxy, and subtracted it from the observed image. To ensure that there are no systematic differences (e.g. due to incompletely corrected high order terms in the ellipse fitting procedure), the residual frame was also filtered to exclude low frequencies. The resulting residual images displaying the detected substructures, caused by dust absorption, are presented in Fig. 1 beside the line emission images. An independent analysis of the continuum image of NGC 2974 was performed using an adaptive filter on the basis of the H–transform (Capaccioli et al. 1988; Lorenz & Richter 1992). The adaptive filtering technique allows a variable smoothing of the image in order to have locally an optimal signal–to–noise ratio. The resulting image of NGC 2974 is shown in Fig. 1.

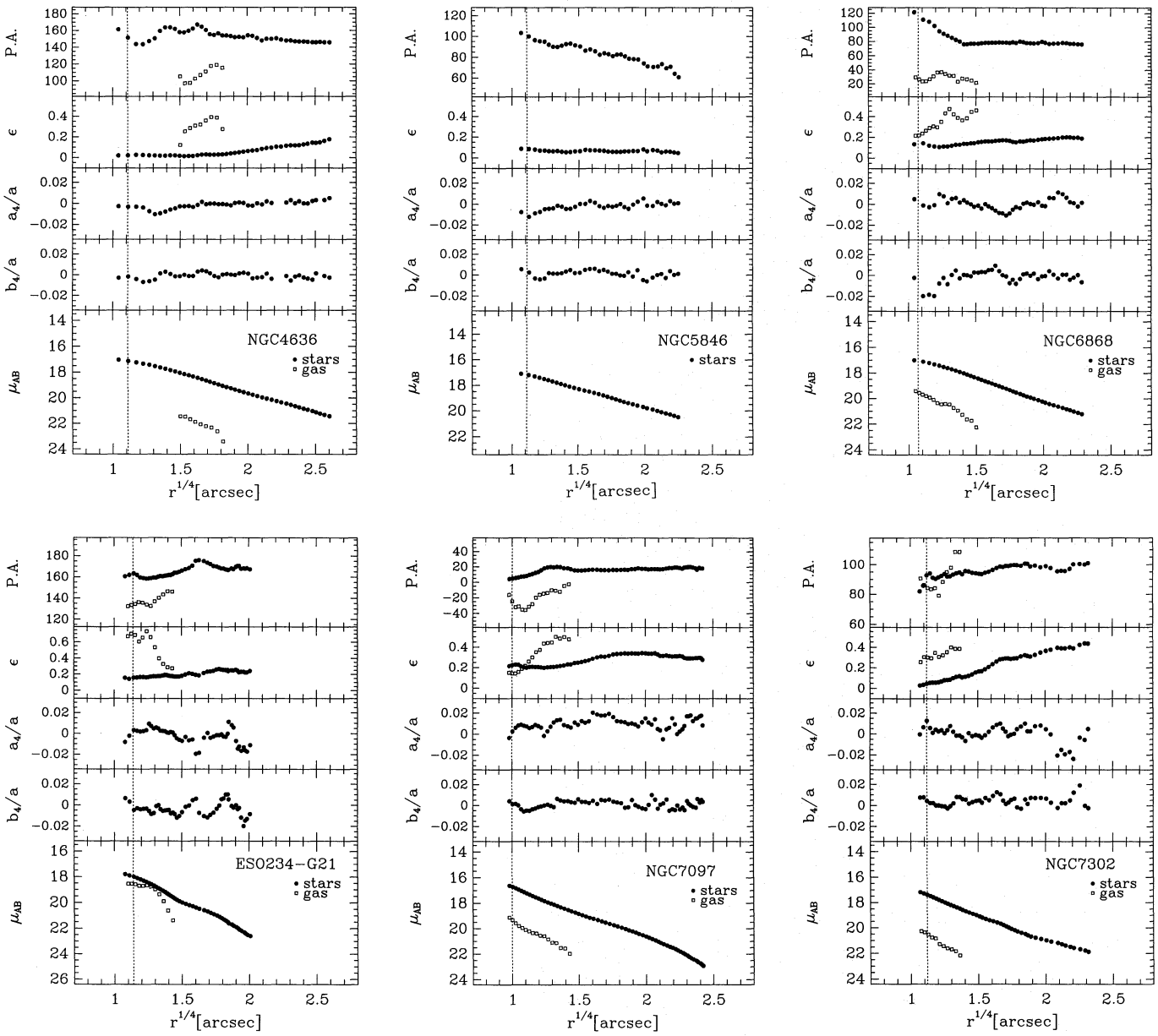

Fig. 2. (continued)

3. The distribution of the ionized gas and stars

Figures 1 and 2 show that in most cases the stellar component of our fifteen galaxies appears regular, with constant ellipticity and little or no isophote twisting (though a few galaxies, such as NGC 5846, do show quite large isophote twists). The isophotes of a few galaxies are slightly *disky*. The line–emitting gas is usually confined to the inner regions and typically extends to 5–15 arcsec from the nucleus. In most cases the gas distribution is also regular, though the major axis of the gas is often significantly misaligned from the stellar figure of the galaxy. The distribution of the projected misalignments between gas and stars for the twelve galaxies with a fundamentally regular gas distribution is given in Fig. 3. The emission–line isophotes are usually significantly flatter than the isophotes of the underlying stellar component. A few of the galaxies show amorphous structures or peculiar (arm–like or ring–like) features in the gas distribution.

We now make some remarks on individual objects in the sample:

NGC 484: The emission is slightly extended in the east–west direction, though confined to the inner regions (r ∼4 arcsec, i.e. ∼2 kpc). The gas is aligned with the stellar body of the galaxy, and its distribution appears regular. The continuum image shows a small major–axis dust lane with about the same extent as the emission region.

NGC 745: The galaxy lies in a group, and has several close companions. The emitting region is quite extended (r ∼5 kpc),

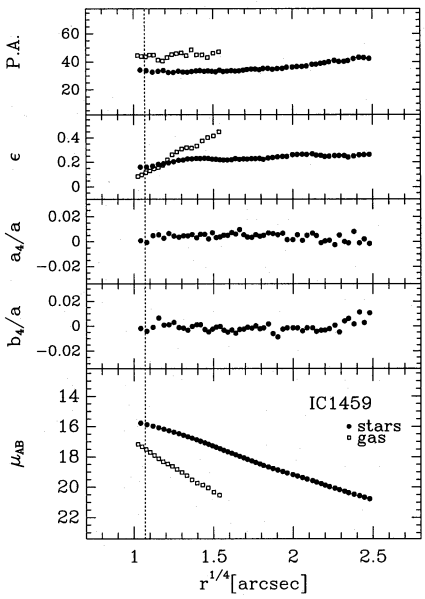

Fig. 2. (continued)

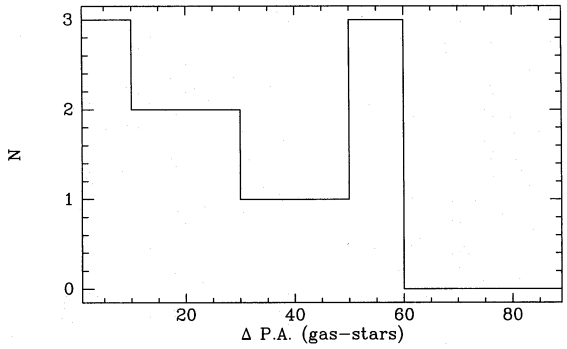

Fig. 3. Histogram of position angle difference for stars and gas in the galaxies in Table 3. NGC 5846 has been excluded because the complex emission–line morphology made it difficult to define the position angle of the major axis

and surrounded by many filaments which extend radially from the centre. There is a possible dust lane along the optical major axis at the position of the emission feature, and some patchy structure near the nucleus.

NGC 1395: The emission region is almost round in the centre and peaked at the nucleus. NGC 1395 is a well–studied elliptical which is both an X–ray source (Canizares et al. 1987) and a shell galaxy (Malin & Carter 1983). Hα+[NII] images have also been obtained by TdiSA and Shields (1991). Lauer (1985) and Véron–Cetty & Véron (1988) found the stellar light to be regular with no optical evidence of dust, though our continuum image suggests there may be a tenuous major–axis dust lane.

NGC 1453: Though confined to the central regions, the emission is strongly decoupled from the stellar component and roughly aligned with the minor axis of the galaxy. The continuum image is smooth, with no obvious features.

ESO 118–G34: This low–luminosity galaxy has an H II region–like emission spectrum (PJDSB) and appears to be actively forming stars. The emission–line image is dominated by several bright H II region complexes. Some of these coincide with 'knots' in the continuum image, though others are seen only in the line image.

NGC 1947: The Hα emission appears to be associated with the complex of dust lanes visible in the continuum light and clearly seen in the galaxy–subtracted image. The line emission extends out to $r \sim 1$ kpc from the center, and several distinct emission–line knots are also visible. The gas velocity field has been studied by Möllenhoff (1982), who estimated the inclination angle of the thin gas and dust disk, giving rise to the observed parallel dust lane structures, to be about 75°. The angular momentum vector of the gas component is orthogonal to that of the stars (Bertola et al. 1992b).

NGC 2974: The ionized gas in this galaxy, which has also been studied by DBB, Kim (1989), TdiSA and Shields (1991), appears to lie in a fundamentally regular elongated structure with some peripheral fainter filaments. The latter could be related to the presence of X-ray emission (Canizares et al. 1987). Kim (1989) noted the presence of a small major–axis dust lane. Analysis of the continuum image using the earlier described adaptive filter reveals a complex substructure with a lens–like feature from which two distinct spiral arm–like structures originate. Schweizer (1992, priv. comm.) and Bregman et al. (1992) also reported evidence for spiral structure in this galaxy. NGC 2974 has also been detected in HI by Kim et al. (1988). These authors note that the HI disk is regular, appears undisturbed and lies along the stellar major axis. The total HI mass is $2\times10^9 M_\odot$ for our adopted distance of 38 Mpc. Perhaps not surprisingly, NGC 2974 also has a faint stellar disk (Scorza 1993; Cinzano & van der Marel 1993).

NGC 3962: The Hα+[N II] emitting region consists of two quite distinct sub–systems: an elongated central component strongly misaligned with both major and minor axes of the stellar figure, and a peculiar, extended arm–like structure departing from the major axis of the internal 'disk' and crossing the stellar body along more than 180°. There are some dust patches in the central region roughly aligned with the emission–line disk.

NGC 4636: This galaxy has an unusual ring–like emitting region extending asymmetrically around the galaxy nucleus. The reality of the gaseous ring is confirmed by (unpublished) spectra taken at several position angles. DBB also noted that the gas in this galaxy had a complex structure, with a 'hole' in the emission–line region at the position of the nucleus. This object has an X–ray halo (Canizares et al. 1987), which may have a central hole (Sarazin 1992, priv. comm.). The optical continuum image reveals a very faint arc–like dust lane extending out to 0.3 R_e and some patchy dust in the central regions.

NGC 5846: This object is an X–ray galaxy (Canizares et al. 1987) and has been observed by DBB, TdiSA and Shields (1991). It shows a complex, filamentary emission–line morphology, including an arm–like feature which resembles the emitting regions of NGC 3962 and NGC 4696 (Sparks et al. 1989). There are also some dust patches associated with the emission region.

NGC 6868: This galaxy shows an elongated emitting region strongly decoupled from the stellar figure and with faint peripheral extensions. A series of dust patches in the centre suggest a skewed dust lane with the same orientation as the ionized gas. Véron–Cetty & Véron (1988) also note the presence of dust in the inner regions, while Hansen et al. (1991) find a central dust lane with weaker spiral–like absorption features extending further out. They remark that the dust distribution closely follows that of Lyα emission–line gas detected with IUE, and suggest that NGC 6868 has recently captured a gas–rich galaxy.

ESO 234–G21: The extended emission of this galaxy is remarkably misaligned from its stellar body. Inside this region the gas appears highly structured, showing a dumb–bell shaped feature. The nearest morphological analogy in our sample is NGC 2974, which shows a bar–like sub–structure in the inner regions. The continuum appears smooth. PJDSB show that the gas kinematics is characteristic of a rotating disk.

NGC 7097: There is an elongated emission region misaligned by $\sim$ 30° with the stellar figure. Some dust is seen along the major axis of the gas disk and in the central regions. Caldwell et al. (1986) have made a detailed dynamical study of NGC 7097 and find that the gas and stars are counter–rotating.

NGC 7302: The emission is slightly elongated with faint patches and/or filaments. There are no conspicuous features in the continuum image.

IC 1459: The emission is roughly aligned with the stellar major axis. Goudfrooij et al. (1990) suggest that the ionized gas disk shows weak spiral structure. Our continuum image shows no conspicuous features, though Goudfrooij et al. report a central red feature in their B–V colour map which appears to be due to dust absorption, and Sparks et al. (1985) also identify IC 1459 as a dusty elliptical. The galaxy is an X-ray source (Canizares et al. 1987). Franx & Illingworth (1988) have shown that IC 1459 has a counter–rotating stellar core confined to the inner 10 arcsec. Since the radial extension of this kinematically decoupled sub-structure matches the size of the elongated emitting region, the origin of the gaseous disk and the counter-rotating stellar core could be related to a merger the galaxy underwent in the past. However, although a sharp change in the slope of the Mg_2 line strength gradient has been observed in the nuclei of other ellipticals with kinematically decoupled cores (Bender & Surma 1992), Carollo et al. (1993) saw no evidence of such a change in the inner 10 arcsec of IC 1459.

4. Discussion

4.1. Structure and distribution of the ionized gas

The geometry of the emitting region in the galaxies observed here suggests that we are generally looking at a fundamentally regular, disk–like structure. The gas is usually strongly concentrated towards the nucleus, with the emission–line intensity dropping more rapidly with radius than the stellar light. Unlike the ionized gas in the disks of spiral galaxies, whose surface brightness follows an exponential law (Kennicutt 1989), the light distribution of these Hα disks shows an $r^{1/4}$–like profile

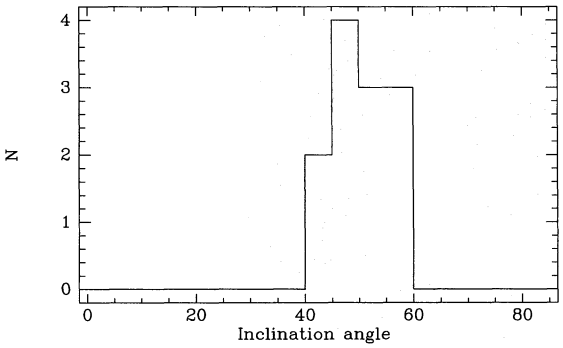

Fig. 4. Distribution of inclination angles for the galaxies of Fig. 3, assuming the gas lies in a circular disk

with a scale length smaller than that of the stellar component. The emission–line isophotes are usually significantly flatter than the isophotes of the underlying stellar component, showing that the gas lies in an inclined disk.

The frequent observation of an ellipticity gradient of the gas disk across the galaxies might result from the presence both of a bar and/or a warp in such disks but if we assume that the disks are essentially flat and circular in shape, the inclination angle i follows from the apparent flattening. The distribution of the inclinations derived from the ellipticities of the outer gaseous disks is shown in Fig. 4. The values range from 40° to 60° (where an edge–on disk has i = 90°). The lack of disks seen close to face–on ($i < 40°$) is not surprising, since these have low surface brightness and would be hard to recognize against the bright background of the underlying elliptical galaxy (this is similar to the problem encountered when attempting to detect faint stellar disks in ellipticals, as noted by e.g., Carter 1987 and Rix & White 1990). Moreover, as mentioned earlier, galaxies with $i > 75°$ will appear as dust–lane ellipticals which were deliberately excluded from the above sample (e.g. NGC 1947).

Gaseous disks within elliptical galaxies are also important for studies of galaxy dynamics. Disks can be used to test the gravitational field of an underlying galaxy and to set strong constraints on the intrinsic shape and orientation of the potential well (Merritt & de Zeeuw 1983; Gerhard & Vietri 1986; Bertola et al. 1991). The calculations are somewhat complex because elliptical galaxies, unlike spirals, are triaxial (Binney 1978, 1985; Franx, Illingworth & de Zeeuw 1991). As a consequence, for a proper description of the system, two axis ratios and two viewing angles must be taken into account, as well as the non–circular shape of the gas orbits. These issues will be addressed in a follow–up paper.

4.2. How much ionized gas is present?

The emission–line luminosity is proportional to the amount of ionized gas present if the electron density and ionization conditions remain constant. If we assume a mean ratio of 1.38 for [N II]/Hα (PJDSB), an electron density of 10^3 cm^{-3} and Case B recombination (Osterbrock 1974; Kim 1989), we find H II masses of a few times 10^3 to a few times 10^5 $M_\odot$ for the galax-

ies of our sample, with a median mass of $6.3\times10^4\ M_\odot$. The estimated mass of ionized gas for each galaxy is given in Table 6.

Figure 5 shows the total ([NII] + Hα) emission–line luminosity $L_{\rm em}$ for the galaxies of the present sample, plotted against absolute magnitude; it also includes data from Kim (1989), Shields (1991) and TdiSA for comparison. The solid line is a linear fit to the PJDSB data for a complete sample of early–type galaxies, calculated with the ASURV package and taking into account upper limits. We find that the early–type galaxies with extended emission–line regions typically have 10 to 100 times as much ionized gas as 'normal' early–type galaxies of the same optical luminosity (the median enhancement is about a factor of 20).[2] An interesting question is whether these galaxies are gas–rich in an overall sense, or simply have a higher fraction of their gas in the ionized component.

4.3. How is the ionized gas related to other components of the ISM?

Macchetto & Sparks (1992) argue that the ionized gas component in early–type galaxies is associated with the cold atomic and molecular component rather than the X–ray component. The observed disk–like morphology of the ionized gas and the presence of dust within the emission regions favour this point of view. In addition, Kim (1989) argues on energetic grounds that the X–ray halo cannot be responsible for the ionized gas observed in individual galaxies other than those at the centres of clusters.

Table 6 lists the masses of gas in the different phases of the ISM (from Roberts et al. 1991 and Knapp et al. 1989) for the 15 galaxies we have observed. The median mass of X–ray gas is $1.5\times10^9 M_\odot$ for the six galaxies observed by the Einstein satellite (Roberts et al. 1991). Since only few direct measurements of atomic and molecular gas are available for these galaxies, we use the dust mass derived from IRAS measurements as a tracer of the cold ISM (Thronson et al. (1989) note however that some of the far–infrared emission in early–type galaxies may be non–thermal). The median dust mass is $8.0\times10^5 M_\odot$, and if we adopt the assumption of Jura et al. (1987) that the dust/gas ratio in elliptical galaxies is similar to that in our own Galaxy, then we find a median HI mass of roughly $8\times10^7 M_\odot$, far higher than the median mass of $6\times10^4 M_\odot$ for the ionized gas.

If the dust (and by implication HI) lies in the same disk as the emission–line gas, then it is important to recognize that the ionized component detected in our images represents less than 1% of the mass in a cold gas disk, and is no more than a tracer of the underlying cold component. This has important implications: it suggests that whether we see an extended emission–line region depends on the ionization conditions rather than the overall gas content of the galaxy, and it may explain why the velocity field of the ionized gas is often regular even when the morphology appears chaotic or disturbed.

4.4. Are these galaxies unusually gas rich?

As noted earlier, the galaxies observed in this program were chosen without reference to their hot or cold gas content. Thus we can ask whether the total gas content is typical of that in early–type galaxies.

For the cold ISM (using the dust as a tracer of atomic and molecular gas), we find a mean ratio $\log[M_{\rm dust}/L_B]$ of -4.68 ± 0.15 for the 11 galaxies in Table 6 which are members of the Roberts et al. (1991) sample, compared with a mean value of -5.07 ± 0.10 for ellipticals and -4.96 ± 0.08 for S0 galaxies in the sample as a whole (Bregman et al. 1992). Thus the dust content of the galaxies we have observed turns out to be a little over twice that of a randomly–chosen set of early–type galaxies.

Analysis of the hot ISM is a little more complex, since both hot gas and discrete sources contribute to the observed X–ray luminosity. However, if we calculate the 'excess X–ray/deficit' parameter used by Bregman et al., we find a mean of $+0.33\pm0.15$ compared with $+0.19\pm0.09$ for the Roberts et al. ellipticals. This again suggests at most a modest enhancement (less than a factor of two) of the hot ISM, but the difference is probably not significant.

Thus although the ionized gas content of the galaxies in Tables 4 and 6 is typically 20 times that expected for a 'normal' early–type galaxy, the overall gas content is not substantially enhanced. It appears that these are galaxies in which a higher than usual fraction of the cold ISM has been ionized, rather than exceptionally gas–rich systems.

4.5. How is the gas ionized?

A complete discussion of the processes by which gas in early–type galaxies is ionized clearly requires spectroscopic data, and is beyond the scope of this paper. However, our data do provide some hints about how galaxies with extended ionized gas disks might differ from other systems.

The linear correlation between emission–line luminosity and stellar luminosity in the large sample of galaxies studied by PJDSB strongly suggests that the dominant ionizing source in 'normal' early–type galaxies is a component of the stellar population, possibly the same (old) stars which are responsible for the upturn in the far–UV flux (Burstein et al. 1988, Greggio & Renzini 1990).[3]

If this is so, then an increase in the emission–line luminosity probably requires a second ionizing source to be present (and dominant) in the galaxies with ionized gas disks. The fact that the gas surface brightness in Fig. 2 usually drops off more rapidly than the stellar light suggests that this second ionizing source is more centrally concentrated than the stellar population.

[2] Although one has to be cautious in comparing the fluxes measured from imaging observations with those from spectroscopic data, the emission–line region was unresolved in most of the galaxies observed by PJDSB and so spectroscopic measurements should reflect the total emission–line flux with a reasonable accuracy.

[3] Photo–ionization by young stars is ruled out except for low–luminosity ellipticals, where it is the dominant ionizing source (PJDSB).

Table 6. Masses of the different ISM components for early–type galaxies with extended emission regions

Galaxy	log $M_{H\ II}$ ($M_\odot$)	log M_{dust} ($M_\odot$)	log M_X ($M_\odot$)	log P_5 (W Hz^{-1})	Notes
NGC 484	5.22	7.06		<22.60	1,2
NGC 745	4.68	6.55		<22.50	1,2
NGC 1395	3.66	5.88	9.29	20.36	3
NGC 1453	5.00	7.02		22.11	3
ESO 118–G34	4.53	5.23		<20.90	1,2
NGC 1947	3.72	5.97	<7.97	20.79	3
NGC 2974	4.50	6.17	8.98	21.11	3
NGC 3962	4.35	<6.34		20.67	3
NGC 4636	4.03	5.51	9.17	21.17	3
NGC 5846	4.40	<6.01	9.82	21.05	3
NGC 6868	4.41	6.36		22.67	3
ESO 234–G21	5.61	6.80		<22.50	1,2
NGC 7097	4.10	5.86		21.68	3
NGC 7302	3.96	<6.69		<21.63	3
IC 1459	4.61	5.43	9.56	23.13	3

Notes:
1. M_{dust} calculated from IRAS fluxes listed by Knapp et al. 1989.
2. P_5 from Sadler et al. 1989, converted to the distance scale adopted here.
3. M_X, M_{dust} and P_5 from Roberts et al. 1991.

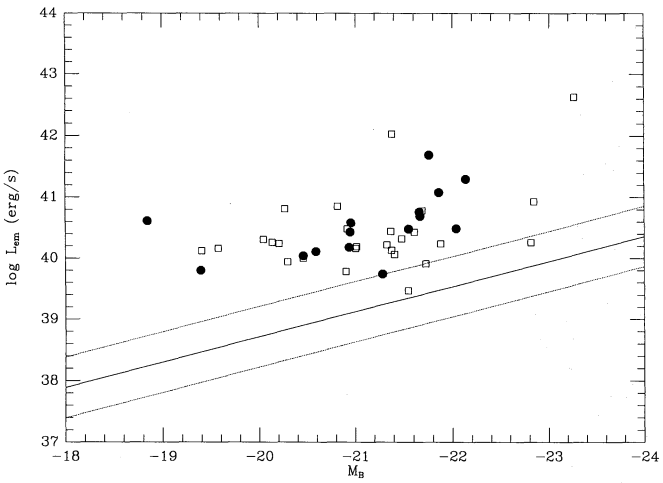

Fig. 5. Comparison of total Hα+[N II] emission–line luminosity for galaxies measured in this study (•), and by Kim (1989), Shields (1991) and TdiSA (□). The solid line shows the mean relation for the complete sample of E and S0 galaxies observed by PJDSB (converted to the distance scale used in this paper). The dotted lines indicate the $\pm 1\sigma$ deviations from the mean

Shields (1991) noted a correlation between emission–line luminosity and 5GHz radio power for the galaxies he observed, but suggested that this might be a selection effect arising from the small size of his sample and the unknown way in which the X–ray emitting galaxies he chose to observe were originally selected. A further complication arises because both radio power and emission–line luminosity are strongly correlated with optical luminosity (Sadler et al. 1989).

To test whether galaxies with ionized gas disks have more powerful radio sources than expected, we define an 'excess radio emission' P_5^{ex}, which is the ratio of the observed radio power P_5 to that expected for an early–type galaxy of the same absolute magnitude based on a linear fit to the data of Sadler et al. (1989):

$$\log P_5^{ex} = \log P_5 + 1.04 M_B + 1.64.$$

The mean value of $\log P_5^{ex}$ is 1.03 ± 0.21 for the 15 galaxies in Table 6, suggesting that the continuum radio powers of galaxies

with ionized gas disks are typically 10–15 times higher than expected. Perhaps the most rigorous test is to take the eight galaxies in Table 6 which belong to the Sadler et al. (1989) sample. Since these are chosen from within a complete sample, and without reference to their radio properties, there should be no selection bias. Though the sample is now very small, it still yields a mean $\log P_5^{\rm ex}$ of 1.62 ± 0.16, implying that the enhancement in radio power is real, is not a selection effect, and is significant at the 5σ level.

We therefore have strong circumstantial evidence that galaxies with extended ionized gas disks are stronger radio sources than other early–type galaxies of similar luminosity, suggesting that an active nucleus plays a part in ionizing the gas disk. This is known to be the case for powerful (FR II) radio galaxies (Baum & Heckman 1989), but the picture is far from simple for less active galaxies because of the lack of any general correlation between emission–line luminosity and radio power (Sadler et al. 1989). Detailed spectroscopic data are probably needed to make further progress.

5. Conclusions

The main conclusions of this study are as follows:

- In most of the 15 E and S0 galaxies studied here, the extended emission–line gas appears to lie in an inclined disk (though kinematical data are needed for a decisive test). The major axes of the stellar and gaseous components are frequently misaligned.
- The mass of ionized gas in these extended disks is typically 10^4–10^5 solar masses, or 10–100 times higher than in 'normal' early–type galaxies of similar optical luminosity.
- The ionized gas is probably closely related to the cold (atomic and molecular) component of the ISM, and may represent much less than 1% of the mass of this component. If so, (i) the kinematics of the ionized gas are likely to be dominated by the underlying cold gas disk and (ii) the amount of ionized gas which is seen will depend on the number of ionizing photons available rather than the amount of gas present.
- The radio continuum emission from early–type galaxies with ionized gas disks is typically ten times more powerful than expected, suggesting that an active nucleus may provide an extra source of ionization.

Acknowledgements. We are indebted to Dr. G. Fasano and to Dr. S. di Serego Alighieri for useful discussions. Werner W. Zeilinger acknowledges the support of the Austrian *Fonds zur Förderung der wissenschaftlichen Forschung* as Erwin Schrödinger Fellow (project nr. J0796–PHY).

References

Amico P., Bertin F., Buson L.M., et al., 1993, A Search for Dark Matter in Elliptical Galaxies: Preliminary Results from an ESO Key Programme. In: Danziger I.J., Zeilinger W.W., Kjär K. (eds.) Structure, Dynamics and Chemical Evolution of Early–Type Galaxies. ESO, Garching, p. 225

Baum S.A., Heckman T., 1989, ApJ 336, 69

Baum S.A., Heckman T., Bridle A., Breugel W.J.M. van, Miley G. 1988, ApJS 68, 643

Baum S.A., Heckman T., Breugel W.J.M. van, 1989, Spectroscopic Observations of Emission Line Gas in Radio Galaxies. In: Meurs E.J.A., Fosbury R.A.E. (eds.) Extranuclear Activity in Galaxies. ESO Workshop, p. 357

Bender R., Möllenhoff C., 1987, A&A 177, 71

Bender R., Surma P., 1992, A&A 258, 250

Bertin G., Bertola F., Buson L.M., Danziger, I.J., Dejonghe, H., Sadler, E.M., Saglia, R.P., Vietri, M., de Zeeuw, P.T., & Zeilinger, W.W., 1989, The Messenger 56, 19

Bertola F., Galletta G., 1978, ApJ, 226, L115.

Bertola F., 1987, Properties of Elliptical Galaxies with Dust Lanes. In: de Zeeuw P.T. (ed.) Proc. IAU Symp. 127, Structure and Dynamics of Elliptical Galaxies. Reidel, Dordrecht, p. 135

Bertola F., Buson L.M., Zeilinger, W.W., 1988, Nature 335, 705

Bertola F., Bettoni D., Danziger J., Sadler, E.M., Sparke, L.S., & de Zeeuw, P.T., 1991, ApJ 373, 369

Bertola F., 1992, Gaseous Disks in Elliptical Galaxies. In: Longo G., Capaccioli M., Busarello G., (eds.) Morphological and Physical Classification of Galaxies. Kluwer Academic Publishers, Dordrecht, p. 115

Bertola F., Buson L.M., Zeilinger, W.W., 1992a, ApJ 401, L79

Bertola F., Galletta G., Zeilinger, W.W., 1992b, A&A, 254, 89

Binney J.J., 1978, Comm. Astroph. 8, 27

Binney J.J., 1985, MNRAS 212, 767

Bregman J.N., Hogg D.E., Roberts M.S., 1992, ApJ, 387, 484

Burstein D., Bertola F., Buson L.M., Faber S.M., Lauer T.R., 1988, ApJ 328, 440

Caldwell N., Kirshner R.P., Richstone D.O., 1986, ApJ 305, 136

Canizares C.R., Fabbiano G., Trinchieri G., 1987, ApJ 312, 503

Capaccioli M., Held E.V., Lorenz H., Richter G.M., Ziener R., 1988, Astron. Nachr. 309, 69

Carollo C.M., Danziger I.J., Buson L., 1993, MNRAS in press

Carter D., 1987, ApJ 312, 514

Cinzano P.A., Marel R.P. van der, 1993, Photometric Disk–Bulge Decomposition, Line Profile Analysis and Dynamical Modeling of the Elliptical Galaxy NGC 2974. In: Danziger I.J., Zeilinger W.W., Kjär K. (eds.) Structure, Dynamics and Chemical Evolution of Early–Type Galaxies. ESO, Garching, p. 105

Demoulin–Ulrich M.-H., Butcher H.R., Boksenberg A., 1984, ApJ 285, 527 (DBB)

de Vaucouleurs G., de Vaucouleurs A., Corwin H.G. Jr., et al., 1991, Third Reference Catalogue of Bright Galaxies. Springer–Verlag, New York (RC3)

di Serego Alighieri S., 1990, Techiniques for Line and Continuum Imaging, In: Longo G., Sedmak G. (eds.) Acquisition, Processing and Archiving of Astronomical Images. OAC, Napoli, p. 311

Ebneter K., Balick B., 1985, AJ 90, 183

Fabbiano G., 1989, A&AR 27, 87

Feigelson E.D., Nelson P.I., 1985, ApJ 293, 192

Forbes D.A., 1991, MNRAS 249, 779

Franx M., Illingworth G.D., 1988, ApJ 327, L55

Franx M., Illingworth G.D., de Zeeuw P.T., 1991, ApJ 383, 112

Gerhard O.E., Vietri M., 1986, MNRAS 223, 377

Gilliotte A., 1990, ESO Filter Inventory. ESO, La Silla

Goudfrooij P., Nørgaard–Nielsen H.U, Hansen L., Jørgensen H.E., de Jong, T., 1990, A&A 228, L9

Greggio L., Renzini A., 1990, ApJ 364, 35

Hansen L., Jørgensen H.E., Nørgaard–Nielsen H.U., 1991, A&A 243, 49
Hawarden T.G., Elson R.A.W., Longmore A.J., Tritton S.B., Corwin H.G., 1981, MNRAS 196, 747
Heckman T.M., Baum S.A., Breugel W.S.M. van, McCarthy P., 1989, ApJ 338, 48
Isobe T., Feigelson E.D., Nelson P.I., 1986, ApJ 306, 490
Jedrezejewski R.I., 1987, MNRAS 226, 747
Jura M., Kim D.-W., Knapp G.R., Guhathakurta P., 1987, A&A 312, L11
Kennicutt, R.C., 1989, ApJ 344, 685
Kim D.-W., Guhathakurta P., Gorkom J.H. van, Jura M., Knapp G.R., 1988, ApJ 330, 684
Kim D.-W., 1989, ApJ 346, 653
Knapp G.R. Turner E.C., Cunniffe P.E., 1985, AJ 90, 454
Knapp G.R., Guhathakurta P., Kim D.–W., Jura, M., 1989, ApJS 70, 387
Kraan–Korteweg R.C., 1986, A&AS, 66, 255
Lauer T.R., 1985, MNRAS 216, 429
LaValley M., Isobe T., Feigelson E.D., 1992. In: Worrall et al. (eds.) Proceedings of the First Annual Conference on Astronomical Data Analysis Software and Systems. Astronomical Society of the Pacific, San Francisco
Lees J.F., Knapp G.R., Rupen M.P., Phillips T.G., 1991, ApJ 379, 177
Lorenz H., Richter G., 1992, Improvement of the Signal to Noise Ratio by Adaptive Filtering, In: Longo G., Capaccioli M., Busarello G. (eds.) Morphologic al and Physical Classification of Galaxies. Kluwer Academic Publishers, Dordrecht, p. 465
Macchetto F., Sparks W.B., 1992, The Warm Component of the ISM of Elliptical Galaxies. In: Longo G., Capaccioli M., Busarello G. (eds.) Morphological and Physical Classification of Galaxies. Kluwer Academic Publishers, Dordrecht, p. 191
Malin D.F., Carter D., 1983, ApJ 274, 534
Merritt D.R., de Zeeuw P.T., 1983, ApJ 267, L19
Möllenhoff, C., 1982, A&A 108, 130
Oke J.B., 1974, ApJS 27, 21
Osterbrock D., 1974, Astrophysics of Gaseous Nebulae. W.A. Freeman and Company, S. Francisco
Phillips M.M., Jenkins C.R., Dopita M.A., Sadler E.M., Binette L., 1986, AJ 91, 1062 (PJDSB)
Rix H.W., White S.D.M., 1990, ApJ 362, 52
Roberts M.S., Hogg D.E., Bregman J.N., Forman W.R., Jones, C., 1991, ApJS 75, 751
Sadler E.M., Jenkins C.R., Kotanyi C.G., 1989, MNRAS 240, 591
Sandage A.R. Tammann G., 1987, A Revised Shapley–Ames Catalog of Bright Galaxies (2nd ed.). Carnegie, Washington (RSA)
Scorza C., 1993, Photometric Properties of Faint Stellar Disks in Elliptical Galaxies. In: Danziger, I.J, Zeilinger W.W., Kjär K. (eds.) Structure, Dynamics and Chemical Evolution of Early–Type Galaxies. ESO, Garching, p. 115
Shields J.C., 1991, AJ 102, 1314
Sparks, W.B., Wall J.V., Thorne D.J., Jorden P.R., Breda I.G. van, Rudd P.J., Jørgensen H.E., 1985, MNRAS 217, 87
Sparks W.B., Macchetto F., Golombek D., 1989, ApJ 345, 153
Sparks W.B., Ford H.C., Kinney A.L., 1993, ApJ, in press
Thomas P.A., Fabian A.C., Arnaud K.A., Forman W., Jones C., 1986, MNRAS 222, 655
Thronson H.A. Jr., Bally K., Hacking P., 1989, Aj 97, 363
Trinchieri G., di Serego Alighieri S., 1991, AJ 101, 1647 (TdiSA)
Véron–Cetty M.-P., Véron P., 1988, A&A 204, 24
White III, R., Sarazin C.L., 1991, ApJ 367, 476

This article was processed by the author using Springer-Verlag LaTeX A&A style file version 3.